

GT2011-46209

ANALYSIS AND EVALUATION OF THE IMPACT OF DIFFERENT BLADE LOADINGS ON
 A 2-STAGE TURBINE WITH SHROUDED BLADES

Dieter Bohn¹, Stephan Schwab²
 Institute of Steam and Gas Turbines
 RWTH Aachen University, Templergraben 55
 52056 Aachen, Germany
 post-bohn@idg.rwth-aachen.de

Michael Sell
 Alstom Power
 Haselstraße 16,
 5401 Baden, Switzerland
 Michael.Sell@power.alstom.com

ABSTRACT

An important goal in the development of turbine bladings is to increase the efficiency in order to achieve an optimized use of energy resources. For that purpose a detailed understanding of flow phenomena is required. This paper presents an experimental investigation of the impact of varying blade loadings on the flow field and leakage flow.

The investigations were conducted on a 2-stage axial turbine at the Institute of Steam- and Gas Turbines, RWTH Aachen University. The flow field for different blade loadings has been determined at the inlet and outlet as well as between the two stages. Consequently, the inhomogeneity at the outlet of each stage, depending on the blade loading, may be investigated. The homogeneity at the outlet has been evaluated by using the secondary kinetic energy coefficient and the formation of the passage vortex has therefore been emphasized. Furthermore, the loading impact on the leakage mass flow and the leakage main flow interaction has been estimated. On this account, the pressure loss in each cavity within the labyrinth seal of the first shrouded rotor blades is detected. The impact on the efficiency of different loadings has moreover been determined. The efficiency has been ascertained by using 5-hole probes and temperature probes after each stage.

The investigations mentioned above have been conducted on a 2D-blade profile and serve as a baseline for future profiled end wall studies. The goal of the endwall contoured blades shall reduce the passage vortex and with it, the under- and overturning which ultimately leads to a more homogeneous outflow from the stage.

NOMENCLATURE

α	Yaw angle	[°]
γ	Pitch angle	[°]
ρ	Density	[kg/m ³]
ψ_h	Enthalpy parameter ($\psi_h = \frac{2\Delta h}{u_{ref}^2}$)	[-]
a	Distance probe-hole to probe end	[mm]

b	Diameter of quasi-3-hole probe	[mm]
c	Absolute velocity	[m/s]
d	Diameter of quasi-3-hole probe	[mm]
h	Enthalpy	[J/kg]
u	Peripheral speed	[m/s]
w	Relative velocity	[m/s]
K	Calibration coefficient	[-]
L	Wall thickness of quasi-3-hole probe	[mm]
p	Pressure	[mbar]

Subscripts

t	Total
s	Static
i	Inlet
m	Mach number

Superscripts

`	Pitchwise mass-averaged value
``	Pitchwise averaged value
0	Pressure “zero“ of the quasi-3-hole probe
1	Pressure “one“ of the quasi-3-hole probe
2	Pressure “two“ of the quasi-3-hole probe

Abbreviations

ave	Averaged
PS	Pressure side
moa	Metal outlet angle
meas	Measured
MP10	Measurement plane upstream of the first stage
MP12	Measurement plane between the two stage
MP22	Measurement plane downstream of the second stage
OP	Operating point
SKE	Secondary kinetic energy
SS	Suction side
DP	Design point

INTRODUCTION

The demand for lower pollutant emission in the field of energy generation requires an improvement of the aerodynamic performance of the blading of turbines. In order

¹ Full Professor, Director
² Research Engineer

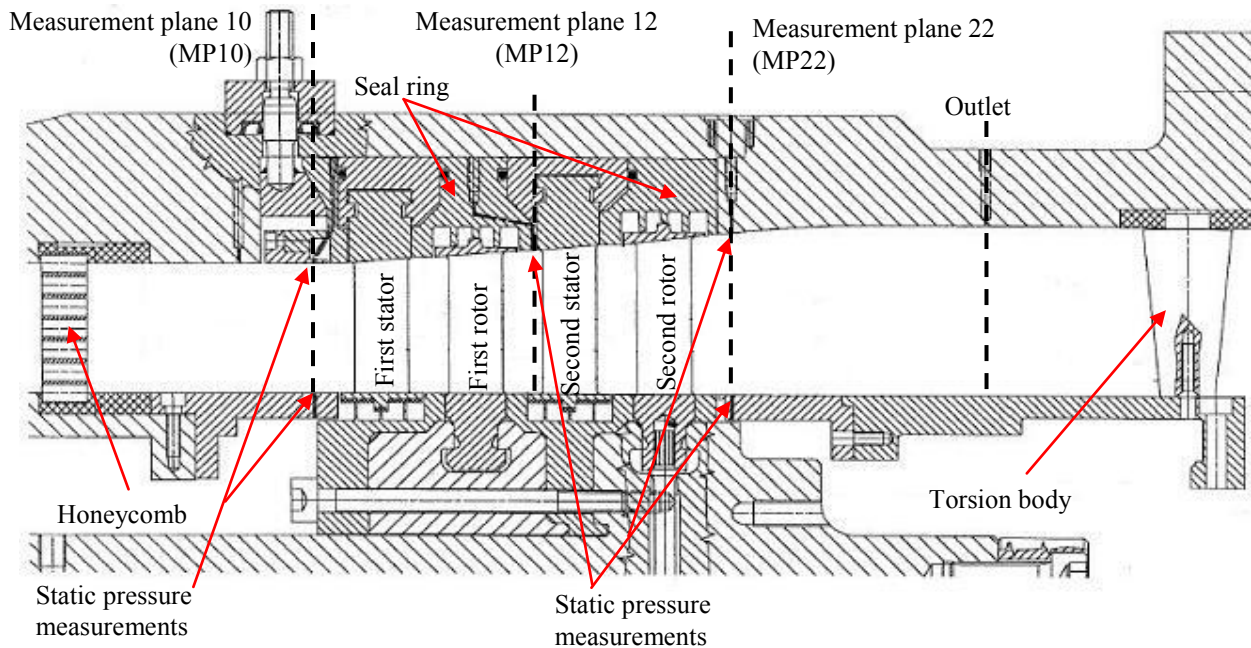


Fig. 1: Cross section of the test rig and measurement planes

to achieve this goal, it is essential to understand the secondary flows. Especially in terms of blades with smaller aspect-ratios these secondary flows are of greater importance. The reinforcement of the passage vortex leads, according to Harvey et al. [1], [2] and Vogt et al. [3], [4], to an enlargement of the exit angle on the side wall (overturning) with a compensating reduction of the downstream flow angle in distance to the side wall (underturning). In doing so, a positive and negative incidence at the inlet of the subsequent stage in the sidewall area is generated and the efficiency is thereby reduced. The load on the sidewall profile section, that is, the pressure difference between suction and pressure side is the major cause of the passage vortex according to Nagel [5]. Weiss et al. [6] have pointed out on a cascade, that an aft-loading causes a reduction of the secondary flow and with it, a loss reduction. In front-loading profiles the passage vortex already arises at the front of the blading and is therefore more pronounced.

Further losses are caused by the leakage flow and its interaction with the main flow. The leakage flow may be significantly reduced with shrouded blades but the flow becomes more complex and the large amount of unsteady flow effects are getting more important. Bohn et al. [7] and Pfau [8] have investigated the back flow area at the inlet and the outlet of the cavity. The strength of these areas is dependent on the incoming mass flow and the latter in turn, on the relative position between the stator and rotor. The leakage mass flow has, according to Pfau et al. [9], much higher entropy than the main flow and generates with reentry inhomogeneities and consequently losses.

The present paper, which may be useful for further end wall studies as it may serve as a baseline, evaluates the effect of different blade loadings on the efficiency of a 2D-blade profile. The goal is to implement an endwall contouring on

this blading by using the results obtained. Thus, the improvements may solely be attributed to the contouring.

TEST TURBINE SET UP

In the experimental setup a 2-stage axial turbine operates at a low pressure ratio of 1.4 with an inlet pressure of $3.2 \cdot 10^5$ Pa and a maximum air mass flow of 12.9 kg/s. The existing test turbine is a scaled model of a steam turbine and operated with air. The air for the test turbine is supplied by 2 electrically driven radial compressors working in parallel mode with a maximum electrical power input of 2.4 MW. To hold the experimental setup at Reynolds and Mach number affinity, the air is pumped in a closed cycle so that the investigations can be done virtually without influence of the environment. The temperatures at the compressor and turbine inlet are controlled by two water driven air coolers. The pressure level in the closed cycle is adjusted by a compression load supply and an exhaust valve. The different loadings are achieved by adjusting the rotation speed by using the water brake. This water brake is integrated into a swing frame which runs in hydrostatic bearings. The rotor power dissipates by means of the water brake which enables a very accurate torque measurement. With the help of the measured torque and rotation speed, the power output may be determined very precisely.

MEASUREMENT SET UP

A broad range of measurement techniques are used in the test rig to measure all flow parameters which are required in order to adjust the operating point. The air mass flow through the turbine is measured upstream at the turbine inlet by using a mass flow nozzle. The mechanical power of the turbine is measured with the aid of the torque momentum and the rotation speed. The torque measurements are realized

using a water brake which is mounted in a momentum pendulum equipped with a torsion arm with load cell.

The flow field inside the turbine is determined upstream of the first row of stator vanes (MP10) and downstream of the second row of rotor blades (MP22) by means of 5-hole and temperature probes with a small recovery coefficient. The pressure distribution as well as the temperature distribution can be measured with the aid of these probes and by using the recovery factor, the static temperature can be determined. Measurements of static pressure inside the casing and at the hub region are also carried out at several axial and circumferential positions. Inlet and outlet temperatures are determined by thermocouple measurements at the inlet honeycomb and the outlet torsion body (see Fig. 1). Table 1 shows the geometric data and operation conditions of the test turbine. The dimensions are related to the hub diameter.

Table 1: Geometric data and operating conditions of the test turbine

Relative average diameter at MP10	[-]	1.17
Relative average diameter at MP22	[-]	1.21
Rel. vane height, stator first stage	[-]	0.17
Rel. vane height, stator second stage	[-]	0.21
Rotor blades / stator vanes	[-]	55 / 55
Inlet absolute pressure	[Pa]	$3.2 \cdot 10^5$
Pressure ratio OP1, OP2, OP3, OP4	[-]	1.4
Enthalpy parameter OP1	[-]	-4.9
Enthalpy parameter OP2	[-]	-3.5
Enthalpy parameter OP3	[-]	-2.7
Enthalpy parameter OP4	[-]	-2.3
Maximal mass flow	[kg/s]	12.9

The two stage stator vanes are fixed in the two inner casings which are in turn independently embedded in an outer casing. The probes are mounted on the outer casing. By traversing the inner turbine casings, the relative position of the probes to the vanes can be changed more than one pitch.

In the measurement plane 12, a temperature probe and a quasi-3-hole probe are inserted in order to measure the flow field. The quasi-3-hole probe has been developed based on the works of Wuest [10], Livesey [11] and Shaw [12] and is illustrated in Fig. 2.

The calibration of the probe was conducted at the institute's own wind tunnel. The wind tunnel, like the test turbine, is operated in a closed mode of operation. This is essential for the compliance with the Reynolds and Mach number affinity.

From the recorded pressure signals, the dimensionless coefficients are formed according to Bohn [13] as follows: yaw (K_α), Mach number (K_m), total (K_t) and static pressure (K_s). The pressures which are required to determine the dimensionless calibration coefficients are measured with a quasi-3-hole probe, in contrast to a conventional 3-hole probe, at different times. By rotating the probe around its own axis the three required pressure information may be obtained (see Fig. 3). Pressure fluctuations are always present during the experimental operation so that the accuracy of determination of the dimensionless coefficient cannot be assured. The pressure values of the probe refer to each

simultaneously measured total pressure at the inlet of the wind tunnel in order to obtain correct identification of the coefficients. On the basis of these coefficients the physical parameters are gained in the experimental operation of the turbine.

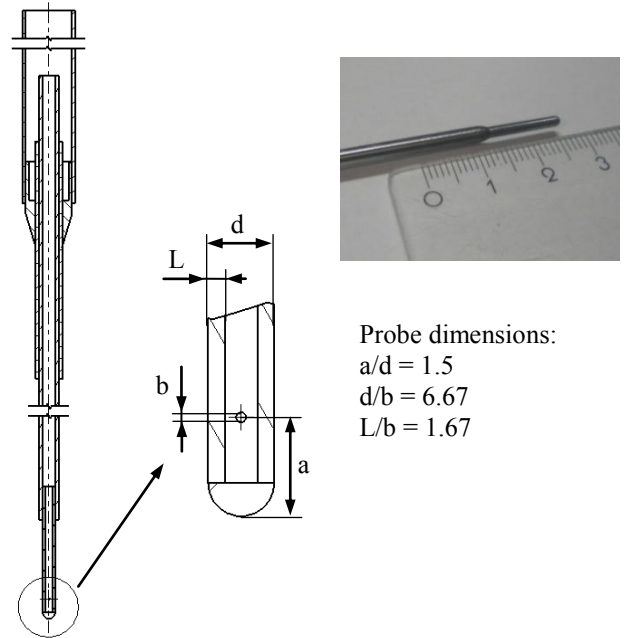


Fig. 2: Quasi-3-hole probe

The pressure values of the probe are, again, based on the simultaneously determined total pressure due to the fluctuation of the operating point. The total pressure used for this purpose is upstream of MP10. The definition of the dimensionless coefficients relating to the total pressure at the inlet of the wind tunnel or rather the inlet of the test turbine is shown in table 2.

Table 2: Dimensionless calibration coefficients

$K_\alpha = \frac{p^1 - p^2}{p_{ti}^1 - p_{ti}^2}$	$K_m = \frac{\Delta p}{p^0}$	$K_t = \frac{p_t^0 - p^0}{p_{ti}^0 - p_{ti}^0}$
$K_s = \frac{p_s^0 - p^0}{p_{ti}^0 - p_{ti}^0}$	where $\Delta p = \frac{p^0}{p_{ti}^0} - \frac{p_{ti}^2 + p_{ti}^1}{2}$	

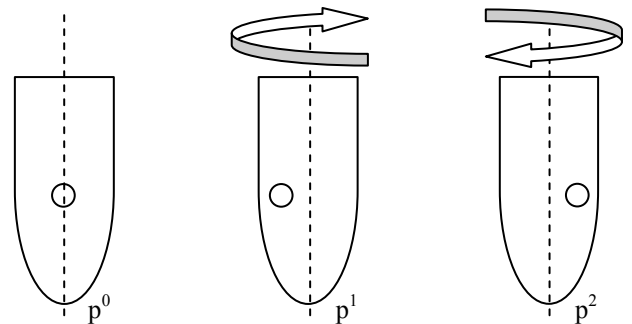


Fig. 3: Measurement concept of a quasi-3-hole probe

For the analysis of the pressure reduction within the labyrinth seal of the first shrouded rotor blade, the pressure has been measured in each cavity on two different peripheral positions. The measuring points, at the same axial position, are displaced by a multiple of half a blade pitch. The radial gap has been measured transiently on two gauges by using an inductive displacement transducer. Fig. 4 demonstrates the gauges mentioned above.

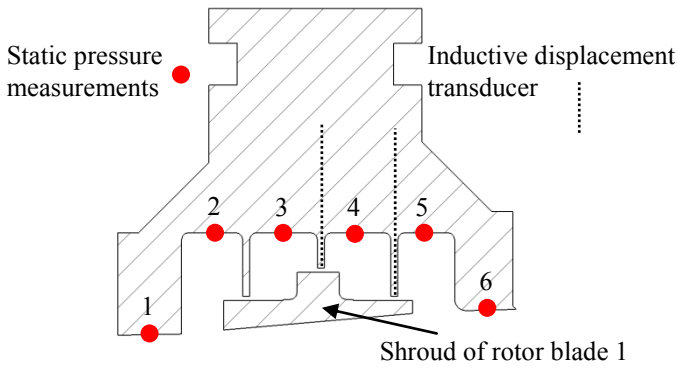


Fig. 4: Measuring points for the analysis of the falling pressure in the cavity and for the determination of the radial gap of rotor 1

At the outlet plane of the turbine four over the circumference evenly divided pneumatic probes are used in order to measure the total pressure. The probes have five fixed metering points on the radial channel height. Due to the different exit angles on the channel height the probes have been constructed with Kiel Heads which are based on Kiel's work [14]. The angular tolerance is for all four pressure rakes at least 87°.

MEASUREMENT RESULTS

Analysis of the flow field and efficiency determination

In order to analyze the effect of varying blade loadings, four different operating points are considered (see Table 1). On the basis of the flow field measurements in MP10, MP12 and MP22 the efficiency for the individual stages and additionally, for both stages is determined depending on the enthalpy parameter. The maximum efficiency is given for $\psi_h = -2.7$ (see Fig. 5), this corresponds to the design point.

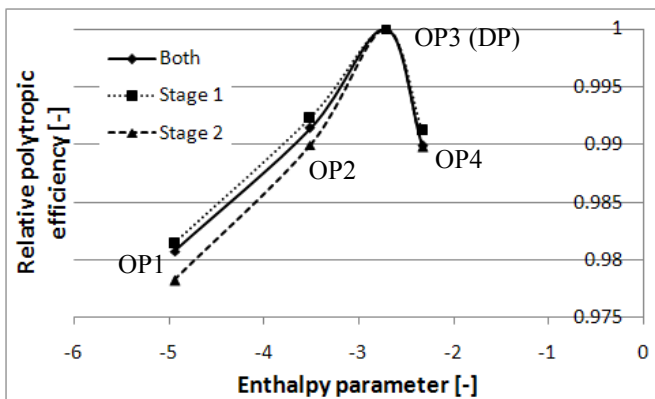


Fig. 5: Relative polytropic efficiency for different operating points

OP2 has a loss of efficiency of 0.9% and OP4 of 1%. In OP4 the blading operates at low loading and flow rating, so that the incidence in this case affects the efficiency negatively.

An important feature of the test rig is that neither the inlet (MP10) nor the probes at MP12, nor the exit plane (MP22) are fixed relative to the inner casing. They are rather fixed respectively to the positions of the blade leading and trailing edges of the prior and following blade rows. This enables a consistent definition of the stage control volume independent of the variable stator-rotor movement. A blade pitch is subdivided into six parts. To make sure that the spectra of all phenomena can be detected, a pitchwise overlap of 120% is added. Due to the reasons of comparability equal inflow must be provided for all operating points. The honeycomb of the turbine ensures a swirl-free flow to the first stage. The pitchwise averaged α'' distribution in the measurement plane 10 shows an angle near 90° for all operating points. The γ'' distribution in the core flow varies between approx. 1° at the hub (10% channel height) and approx. 9° on the casing (90% channel height) (see Fig. 6). This change occurs due to incipient enlargement of the flow channel (cylindrical hub and conical casing). The relatively large deviations of the outermost data points are caused by the probe head-wall-interaction.

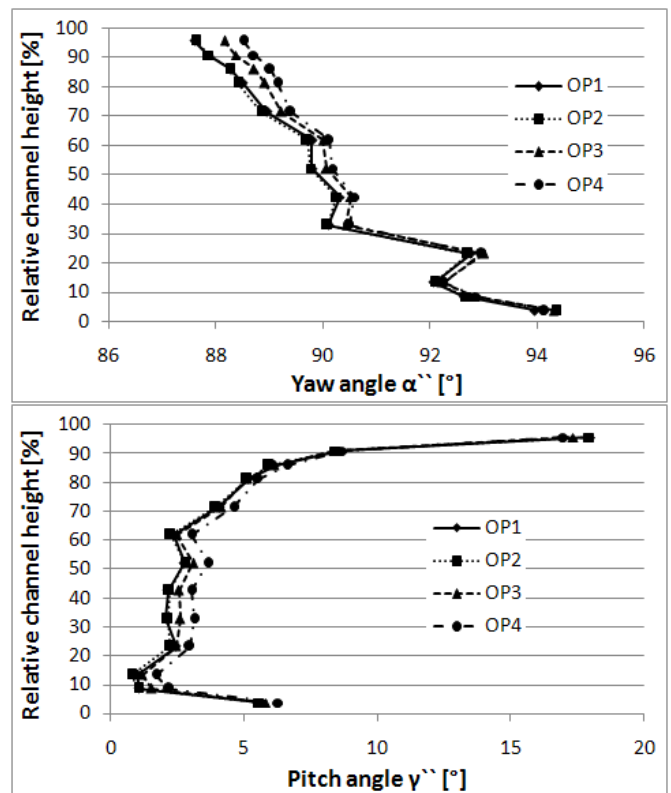


Fig. 6: α'' (above) and γ'' (below) distribution in MP10

The α distribution against the circumferential position and the operating points is illustrated in Fig. 7 (a) for MP12 and Fig. 7 (c) for MP22. The yaw angle is defined as follows: 90° is swirl-free and above 90° is counter-swirl.

For operating point one an outflow with a strong counter-swirl for both measurement planes is given. The out-

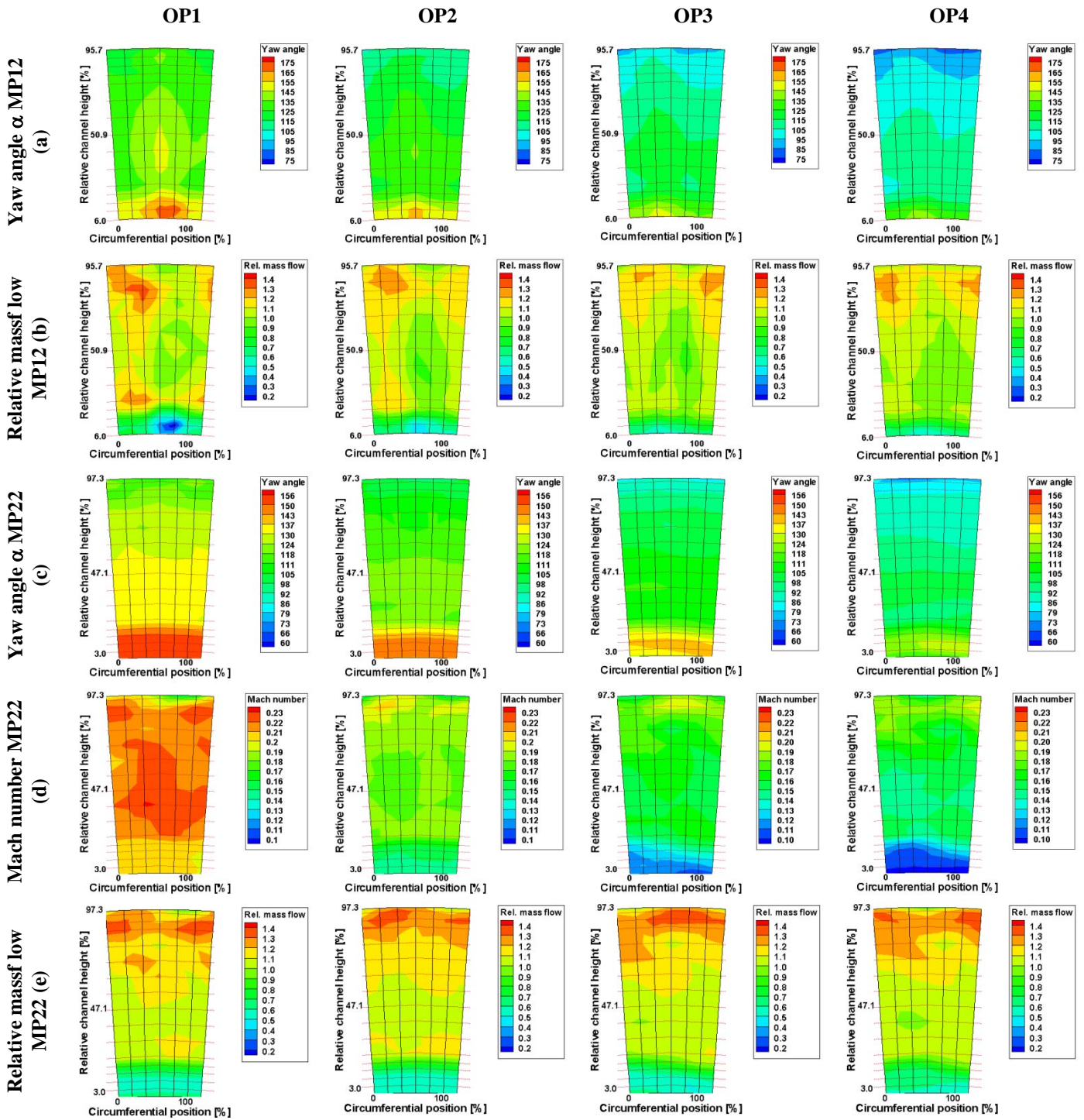


Fig. 7: Results of field measurement in MP12 and MP22

flow, however, becomes steadily smaller due to increasing rotation speed in the other operating points. For the operating point four a Co-swirl above 70% is given. From 25% (MP12) or rather from 30% (MP22) of the relative channel height discontinuities are noticeable in the absolute outflow which are caused by the casing-side passage vortex. For operating points one and two an overturning takes place at 60% (0.9° related to the leading edge of stator two, located at the suction side) and 80% (0.4° related to the leading edge of stator two, located at the pressure side) of the circumferential position at the hub region which is caused by the potential

effect of the subsequent stator. This repercussion on the yaw angle is reduced with increasing operating points and is only very weakly present in OP4. In accordance with the overturning, the relative mass flow at these positions is also reduced.

The relative mass flow is obtained for each operating point to the respective maximum in the channel, so that the homogeneity of the operating points can be compared. Due to the constant pressure ratio and the increasing rotation speed the absolute mass flow decreases from OP1 to OP4 by 4 %. It appears, that with decreasing blade loading a more

homogeneous distribution is achieved which is especially evident behind rotor 1 on MP12 (see Fig. 7 (b)). The differences on MP22 (see Fig. 7 (e)) between the operating points are no longer as pronounced and also the previously mentioned effect is inexistent as there is no subsequent stator blade given.

The average Mach number decreases with increasing rotation speed which is the result of the decreasing amount of the absolute speed. The Mach number drops off sharply for MP22 below 23% of the channel height (see Fig. 7 (d)). This decline is most pronounced at low blade loading and decreases with increasing blade loading. The decline is also apparent in MP12 but less pronounced (18% channel height, which is cannot be seen in Fig. 7). These effects occur due to the passage vortex. For the detailed analysis of the passage vortex a determination of the secondary kinetic energy is useful which allows a qualitative assessment of the losses. For the SKE, the relative outflow of both rotors of stage one and two are considered. From the difference of the metal outlet angle to the measured relative outflow angle, the secondary velocities with equation (1) may be calculated.

$$\vec{w}_{SKE} = \vec{w}_{meas} - \vec{w}_{met} \quad (1)$$

As a gauge of the secondary losses the kinetic energy of the secondary velocity may be used. In order to allow a comparison of different operating points, the secondary energy refers to the kinetic energy of MP10 in the meridonal section [equations (2) and (3)].

$$SKE = \frac{1}{2} w_{SKE}^2 \quad (2)$$

$$w_{SKE} = \frac{SKE}{0.5 c_{MP10}^2} \quad (3)$$

The SKE coefficient for MP12 and MP22 is illustrated in Fig. 8. The secondary kinetic energy within the outflow area of rotor blade 1 is between 30 to 70% very marginal. From 15 to 30% of the channel height is a slight increase in the secondary energy, in consequence of a minor overturning which is caused by the passage vortex. A very pronounced secondary energy becomes apparent below 20% for OP1 and OP2 and 15% for OP3 and OP4 of the channel height as the passage vortex causes this time an overturning. In both cases, the secondary energy rises up to OP3. The passage vortex is less pronounced in the casing area.

The secondary energy in the outflow area of the rotor blade 2 is all in all greater, especially in the casing area but also in the center of the channel. In this connection, the inhomogeneous flow has to be considered. In the hub region is the increase of the secondary energy, caused by the passage vortex, also evident which goes in this case up to 40%. The maximum intensity however is fading, especially on OP1 from MP12 to MP22 that results from a smaller blade loading of the second stage. It is reduced, in comparison to the first stage, in OP1 by 10% and in OP4 by 6% which leads to a lower cross pressure gradient.

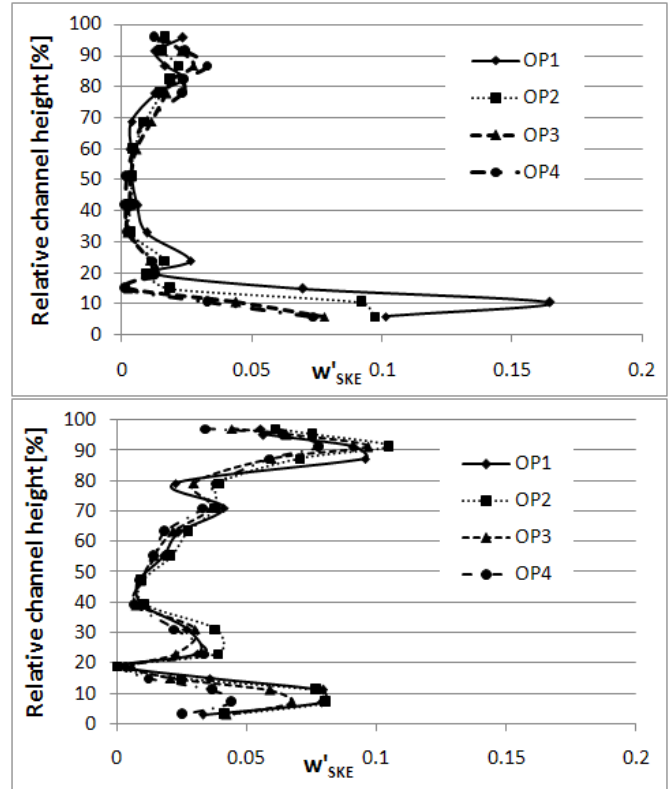


Fig. 8: Secondary kinetic energy coefficient for MP12 (above) and MP22 (below) in dependency on the operating point

Analysis of the leakage flow

The pitchwise averaged static pressure rises along with the decrease of the blade loading. Due to the higher rotation speed the degree of reaction in the first stage rises, causing a decrease of the pressure in the first stator at the measuring point 1. The pressure distribution in the labyrinth and corresponding to the measurement position in Fig. 4, are portrayed in Fig. 9. The measured static pressure in the labyrinth is related to the dynamic pressure in measurement plane 10 and is called, in the following, relative static pressure. The relative static pressure in Fig. 9 is pitchwise averaged.

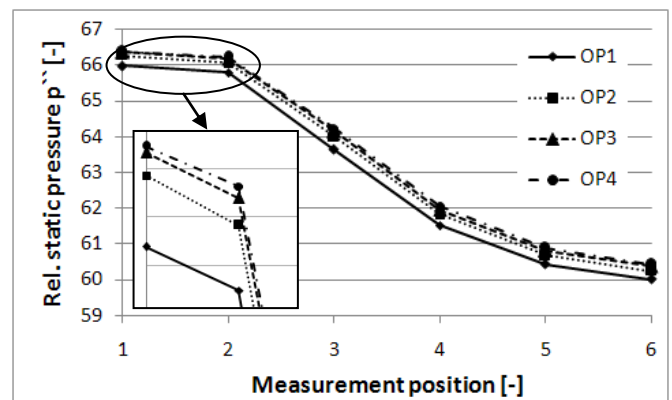


Fig. 9: Relative pressure loss in the labyrinth of rotor one

The pressure reduction within the labyrinth seal, from the metering point two to five differs in all operating points by 2 mbar and may therefore be assumed to be constant. The

pressure reduction of the leakage mass flow is an elementary size and therefore only minimal distinctions of the leakage mass flow are to be expected. Since the leakage mass flow depends on the specific volume at the inlet, the leakage mass flow should rise with increasing blade loading. Since, however the different blade loadings are generated by an alteration of the rotation speed, a reduction of the radial gap due to centrifugal force, is caused. This is to be seen in Fig. 10.

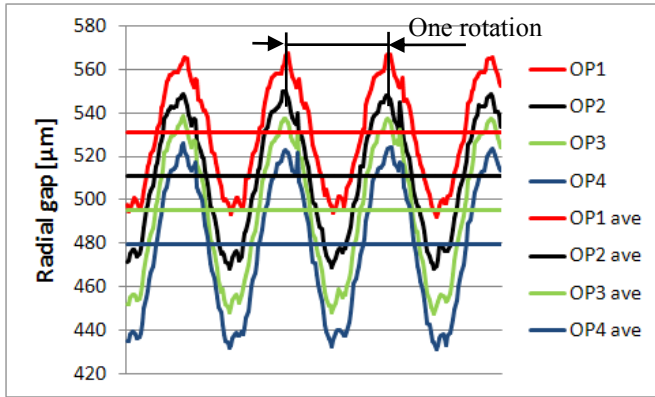


Fig. 10: Transient determined radial gap and average value

Measurements were conducted in the two positions as demonstrated in Fig. 4 for reasons of comparability. By reference to these information the relative leakage mass flow may be obtained. To calculate the leakage flow, two different models of Stodola were used which are summarized in Traupel [15]. Table 3 shows that the leakage mass flow changes only marginally from the cavity of stator one.

Table 3: Relative leakage mass flow

OP	1	2	3	4
Theoretical and empirical model by Stodola	1.063%	1.052%	1.036%	1.008%
Stodola	0.975%	0.934%	0.948%	0.914%

While the pressures in the cavity are independent from the position of the stator blade, dependencies at the inlet and outlet become apparent. When entering into cavity, the pressure fluctuations are approximately equal for all four operating points and are characterized by a peak behind the trailing edge of stator blade one and by a minimum in the channel (see Fig. 11). The average values of the pressures at the inlet show an increase, due to the rising degree of reaction (see Fig. 9). The measuring point with the highest pressure is located in the extension of the blade mean lines of stator blade one. The increase in pressure at this point originates from the wake of stator blade one.

At the outlet of the cavity a shift from the maximum pressure to the pressure side with increasing blade loading becomes obvious (see Fig. 12). The absolute outlet flow angle rises with decreasing peripheral speed which leads to a positive incidence of subsequent stator blades. Thereby the potential field is shifted.

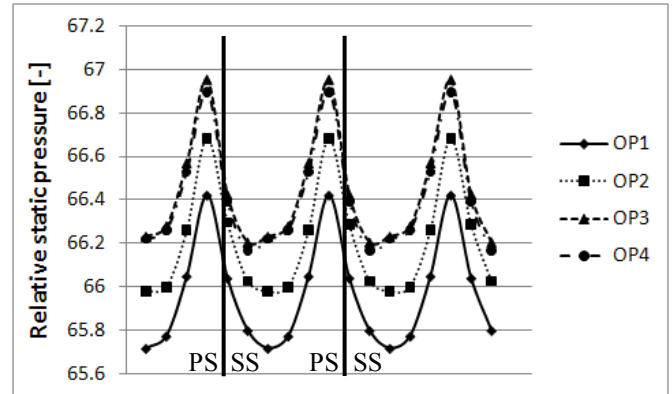


Fig. 11: Pressure fluctuations at the inlet of the cavity in dependence on the stator position

The inhomogeneities on the wall of the blade channel are more pronounced due to the shift of the potential field and the positive incidence at high blade loading. Thus, at the outlet, in opposition to inlet (see Fig. 11), of the cavity of rotor blade one are the pressure fluctuations in dependence on the blade loading. The pressure difference however increases, depending on the stator blade position, from the last cavity to the outlet of the cavity (see Fig. 4 measuring point 5 and 6). Therefore it is anticipated that the leakage jet leaks with more energy in the flow channel and causes higher losses. Thus, the average pressure is an indication of how powerful the leakage mass flow enters into the main flow channel. According to that is the fluctuation of the leakage jet most pronounced on OP1.

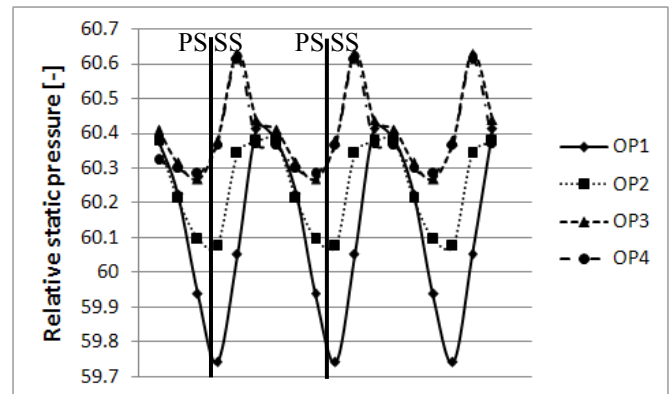


Fig. 12: Pressure fluctuations at the outlet of the cavity in dependence on the stator position

CONCLUSION

The effect of varying blade loadings has been investigated. The outflow from the first stage is, above 20% of the channel height, homogeneous. Below this 20%, the secondary energy increases sharply with rising blade loading and is expanding, within the outflow area of the second rotor blade, over the entire channel. A reduction of the passage vortex at the hub of rotor one will improve the flow conditions in MP22. This reduction may be achieved by an endwall contouring in the hub- and casing area. The contouring has to be placed over the entire axial length of the blade. The aim of the endwall contouring is the guidance of the side wall boundary layer. For that purpose, the velocity is

reduced in the front of the blade by a dent on the side wall. The boundary layer, due to its low momentum, is transported more to the suction side. By a subsequent increase of the side wall the side wall boundary layer is accelerated and oriented according to the channel path. Thus, lesser way for material exchange with the boundary layer is available and the passage vortex develops to a lesser extent that consequently leads to a more homogeneous outflow out of the stage.

For future investigations the inspected bladings will be extended by an endwall contouring at the shroud as well as the blade root, which will happen with the help of the company Alstom. The changes of the flow conditions therefore result solely from the endwall contouring. Since it is a 2D profile, the potential of the endwall contouring can be assessed accurately. This paper may also serve as a guideline to support further profiled end wall studies.

ACKNOWLEDGMENTS

The experimental investigations were conducted as part of the joint research program COORETEC-turbo in AG Turbo. The work was supported by the Bundesministerium für Wirtschaft und Technologie (BMWi) under file number 0327716R on the basis of a resolution of the German Parliament. The authors gratefully acknowledge AG Turbo, MTU Aero Engines and Alstom Power for their support and permission to publish this paper. The responsibility for the content of this publication lies with the authors.

REFERENCES

- [1] Harvey, N. W., Rose, M. G., Taylor, M. D., Shahpar, S., Hartland, J., and Gregory-Smith, D. G., 2000, "Nonaxisymmetric Turbine End Wall Design: Part I - Three-Dimensional Linear Design System," *Journal of Turbomachinery*, pp. 278-285
- [2] Harvey, N. W., Brennan, G., Newman, D. A., and Rose, M. G., 2002, "Improving Turbine Efficiency Using Non-Axisymmetric End Walls: Validation in the Multi-Row Environment and with Low Aspect Ratio Blading," *ASME Paper No. GT-2002-30337*
- [3] Vogt, H.-F., 2000, "Influence of non-axisymmetric endwalls on the secondary flows in annular turbine cascades: Visualization in a water channel," *Forschung im Ingenieurwesen* 65, pp. 247-256
- [4] Vogt, H.-F., and Zippel, M., 1996, "Sekundärströmungen in Turbinengittern mit geraden und gekrümmten Schaufeln; Visualisierung im ebenen Wasserkanal," *Forschung im Ingenieurwesen - Engineering Research*, pp. 247-253
- [5] Nagel, M. G., 2004, "Numerische Optimierung dreidimensional parametrisierter Turbinenschaufeln mit umfangunsymmetrischen Plattformen - Entwicklung, Anwendung und Validierung," Ph. D. thesis, University of the Federal Armed Forces Munich
- [6] Weiss, A. P., and Fottner, L., 1995, "The influence of Load Distribution on the Secondary Flow in Straight Turbine Cascades," *Journal of Turbomachinery*, Vol. 117, pp. 133-141
- [7] Bohn, D., Ren, J., Tümmers, C., and Sell, M., 2005, "Unsteady 3D-Numerical Investigation of the Influence of the Shroud Cavities on the Stator-Rotor Interaction in a 2-Stage Turbine," *ISABE Paper No. 2005-1155*
- [8] Pfau, A., 2003, "Loss Mechanisms in Labyrinth Seals of Shrouded Axial Turbines," Ph. D. thesis, Swiss Federal Institute of Technology Zurich
- [9] Pfau, A., Treiber, M., Sell, M., and Gyarmathy, G., 2000, "Flow Interaction From the Exit Cavity of an Axial Turbine Blade Row Labyrinth Seal," *ASME Paper No. 2000-GT-481*
- [10] Wuest, W., 1963, "Eigenschaften von Zylindersonden zur Strömungsmessung," *Zeitschrift für Instrumentenkunde*, 71. Jahrgang, Heft 7
- [11] Livesey, J. L., 1956, "The behavior of transverse cylindrical and forward-facing total pressure probes in transverse total-pressure gradients," *J. aero. Sci.* 23, p. 949
- [12] Shaw, R., 1960, "The influence of hole dimension on static pressure measurements," *J. Fluid Mech.* 7, 4, pp. 550-564
- [13] Bohn, D., and Simon, H., 1975, "Mehrparametrische Approximation der Eichräume und Eichflächen von Unterschall- bzw. Überschall-5-Loch-Sonden," *Archiv Technisches Messen*, pp. R31-R37
- [14] Kiel, G., 1935, "Gesamtdruckgeräte mit großer Unempfindlichkeit gegen Schräganströmung," *Bericht der Deutschen Versuchsanstalt für Luftfahrt*, e. V., Band 12, pp. 75-79
- [15] Traupel, W., 1988, "Thermische Turbomaschinen," Version 1, 3. Revised and extended edition, Springer-Verlag Berlin, Heidelberg, New York, London, Paris, Tokyo